

Multiscale Detection of Filamentary Features in Image Data

Xiaoming Huo¹, Jihong Chen¹, David Donoho²,
¹ Georgia Institute of Technology, Atlanta, GA 30332,
² Stanford University, Stanford, CA 94305

July 31, 2003

Abstract

Taking advantage of the new developments in mathematical statistics, a multiscale approach is designed to detect filament or filament-like features in noisy images. The major contribution is to introduce a general framework in cases when the data is digital. Our detection method can detect the presence of an underlying curvilinear feature with the lowest possible strength that are still detectible in theory. Simulation results on synthetic data will be reported to illustrate its effectiveness in finite digital situations.

Keywords: Multiscale detection of filamentary structures, Digital image, Curvilinear features, Digital axoids.

Acknowledgement

This work is partially supported by NSF DMS 01-40587 and 01-40698.

1 Introduction

Detecting the presence of a filament (or a filament-like feature) in a noisy picture is a fundamental problem in many applications, such as medical image processing, target recognition, satellite image analysis, and many more.

Recently, there has been significant advances in mathematical statistics on this problem. Namely, in [1], it is proven (as one of many cases) that when the underlying features is a digitized line segment, when the amplitude of the signal residing on the underlying feature is strong enough, there is a statistical means to reliably detect it. If the amplitude of the signal is not strong enough, which can be quantified, then there is no method that can detect it. Moreover, there is an algorithm that achieves the lowest possible order of complexity. The fundamental tools that are used is introduced in [4].

To detect a filamentary feature, which is more likely to be *curvilinear*, the previous result, which requires *straight* line segment, is not strong enough. In a working paper [3], for point processes (note: not imagery data), it is shown that the number of points on a smooth function is governed by certain laws. This result gives the possibility to calculate the detectability of an underlying curvilinear feature in a point process. In addition, even though the result from point processes can *not* be directly applied to imagery data, the

developed techniques – covering and the related probabilistic analysis – can be adapted for the digital problem.

Our method is directly inspired by a very similar approach in [2]. The main differences are (1) the continuous axoids are replaced by digital axoids, and (2) the distribution for a point process is replaced by a distribution of intensities at pixels.

The proposed method is capable of detecting underlying features with arbitrary location, orientation, and scale as long as the amplitude, smoothness, and the anisotropic ratio satisfy certain conditions, which are very general.

The major contribution of this paper is to describe in details a multiscale framework to detect the presence of a filamentary feature in digital noisy images.

The rest of the paper is organized as follows. In Section 2, the formulation of the problem is given. In Section 3, we describe the structure of digital axoids. In Section 4, a detection method based on statistical hypothesis testing is introduced. In Section 5, simulation results are used to demonstrate the effectiveness of our method. Finally, some discussion and concluding marks are provided in Section 6.

2 Formulation

The formulation for image data is given in Section 2.1. In Section 2.2, some remarks are given.

2.1 Image Data

Image data are $x(i, j)$, $1 \leq i, j \leq n$, where one normally assume that n is dyadic: $n = 2^J$. The value of $x(i, j)$ is equal to the intensity at pixel (i, j) .

An underlying feature can be considered as a subset of pixels: $F = \{(i, j)\}$. Let $|F|$ denote the cardinality of the set: i.e. the number of pixels in F . This subset of pixels will follow some conditions. For example, the following is an analogy of the Lipschitz condition for continuous functions.

Condition 2.1 *There exist C and M , such that for pixels (i_1, j_1) and (i_2, j_2) , $|i_1 - i_2| < M$, we have*

$$\max_{j_1, j_2} \{|j_1 - j_2| : (i_1, j_1), (i_2, j_2) \in F\} \leq C|i_1 - i_2|.$$

Apparently, the above condition only allows the height of a feature to be 1. The above condition can be generalized to include the feature whose height (which sometimes is called thickness) is larger than 1, by considering the lower and upper boundary of the feature. In this paper, we leave it as an exercise for readers.

The image data can be considered as a realization of a Gaussian random field, namely:

$$x(i, j) \sim \begin{cases} N(0, 1), & \text{when } (i, j) \notin F, \\ N(A_n, 1), & \text{when } (i, j) \in F, \end{cases} \quad (1)$$

where A_n is a constant.

The fundamental questions are what the pair (F, A_n) should be so that the underlying feature becomes detectable, and if it is detectable, what an efficient numerical method will be?

2.2 Discussion

We would like to make a few comments before describing the data structure.

1. First of all, for point processes, the above problems (from a theoretical point of view) has been answered in [3] and [2].
2. More general conditions can be introduced, to cover more generic digital curves. For example, Condition 2.1 mimics the Lipschitz condition. We may later introduce a condition which mimics the Hölder condition.
3. This paper will emphasize the computational framework, instead of the theoretical aspect of this problem.
4. In many existing works, the feature F is introduced as a discretization of a continuous object. For simplicity, we avoid that kind of description.

3 Digital Axoids, Significance Graph, and the Longest Paths

The motivation of defining our data structure is summarized in Section 3.1. In Section 3.2, definitions of *digital strips* are given. In Section 3.3, we define the *significance graph*. In Section 3.4, the conditions of *good continuation* is given. Finally, the *longest run* is explained in Section 3.5. The concepts that are described here is nearly parallel to the ideas that were described in [2].

3.1 Motivation

Recall that a fundamental idea that is embedded in the approach of [3] and [2] is to design some basic objects, such that an underlying feature can be efficiently covered by a small set of these basic objects. In [3], these basic objects are rectangles or slanted rectangles. In [2], they are dyadic axoids (which is also called strips).

The detection of an underlying feature is based on the following phenomena:

1. When there is *no* underlying object, some statistics associated with the basic objects can ‘hardly’ exceed a prescribed threshold. We say a basic object becomes significant if and only if its statistic exceeds the threshold. Consequently it will be ‘rare’ to see a chain of continuous significant basic objects.
2. When there is an underlying object and the associated amplitude A_n is ‘significantly’ large, the statistics on the basic objects that ‘mostly’ overlaps with the underlying feature are most likely to exceed a prescribed threshold. Consequently it is likely to have a ‘long’ chain of continuous and significant basic objects.

Utilizing the above facts, a detection scheme can be designed. The detection statistic will be based on the length of the *longest path* (or *longest run*).

There is one more level of difficulty embedded. Namely if one considers a straight line feature, then a beamlet-like scheme that is described in [4] and [1] can provide an efficient solution. However, this approach fails when the underlying feature could be curvilinear. To remedy this, the approach in [2] is to consider basic objects at a range of scales. It is

proven that there exists a scale at which there is a ‘good covering’ of a potentially curvilinear feature. And then a longest path statistic can be used to detect the presence. Note that at different scales, the basic objects have different width and height (i.e., thickness). This is indeed a multiscale methodology. It is shown in [2] that such an approach can cope with a range of smoothness (or regularity) conditions for the underlying features. Comparing with a beamlet-like method, the new method can be considered as a method that uses thickened beamlets.

In the next section, we describe our basic objects: *digital axoids*.

3.2 Digital Axoids

As mentioned earlier, the digital axoids are derived from the dyadic strips in [2].

First of all, a scale $s, s = 1, 2, \dots, J$, is fixed. Practically, we may impose $1 < s$ and $s < J$.

The $n \times n$ image is divided into 2^s vertical strips; each strip is an $n \times 2^{J-s}$ subimage. Let $k = 1, 2, \dots, 2^s$, be the index of these vertical strips. For a fixed k , let $\ell_0 (\ell_0 = 1, 2, \dots, n)$ denote a row number in the vertical strip, Let $\ell_0 + \ell_1$ ($1 \leq \ell_0 + \ell_1 \leq n$, and $-S \cdot 2^{J-s} \leq \ell_1 \leq S \cdot 2^{J-s}$, where S is a prescribed constant) denote another row number. Between pixels $((k-1) \cdot 2^{J-s} + 1, \ell_0)$ and $(k \cdot 2^{J-s}, \ell_0 + \ell_1)$, there is a digital line determined by the Bresenham’s line drawing algorithm. Let $B(\cdot)$ denote a function such that the pixel set

$$\{(i, B(i)) : (k-1) \cdot 2^{J-s} + 1 \leq i \leq k \cdot 2^{J-s}\}$$

are the pixels that made the Bresenham’s line. A *digital axoid* is a set of pixels that thickens such a line, formally, the following set of pixels

$$a(s, k, \ell_0, \ell_1) = \left\{ (i, j) : \left| \begin{array}{l} (k-1) \cdot 2^{J-s} + 1 \leq i \leq k \cdot 2^{J-s}, \\ \max\{1, B(i) - 2^{s-1}\} \leq j \leq \min\{B(i) - 1 + 2^{s-1}, n\} \end{array} \right. \right\}$$

form a *digital axoid*.

In Figure 1, digital axoids (for an 8×8 image) at different scales and positions are presented.

3.3 Significance Graph

For a given digital axoid $a(s, k, \ell_0, \ell_1)$, a statistic can be defined as follows:

$$X(s, k, \ell_0, \ell_1) = \frac{1}{\sqrt{n}} \sum_{(i,j) \in a(s,k,\ell_0,\ell_1)} x(i, j).$$

When this digital axoid does not overlap with the underlying feature, i.e., $a(s, k, \ell_0, \ell_1) \cap F = \emptyset$, one can easily derive

$$X(s, k, \ell_0, \ell_1) \sim N(0, 1).$$

When there is an intersection ($|a(s, k, \ell_0, \ell_1) \cap F| > 0$, where $|a(s, k, \ell_0, \ell_1) \cap F|$ is the number of ‘common’ pixels), we have

$$X(s, k, \ell_0, \ell_1) \sim N\left(\frac{1}{\sqrt{n}} |a(s, k, \ell_0, \ell_1) \cap F|, 1\right).$$

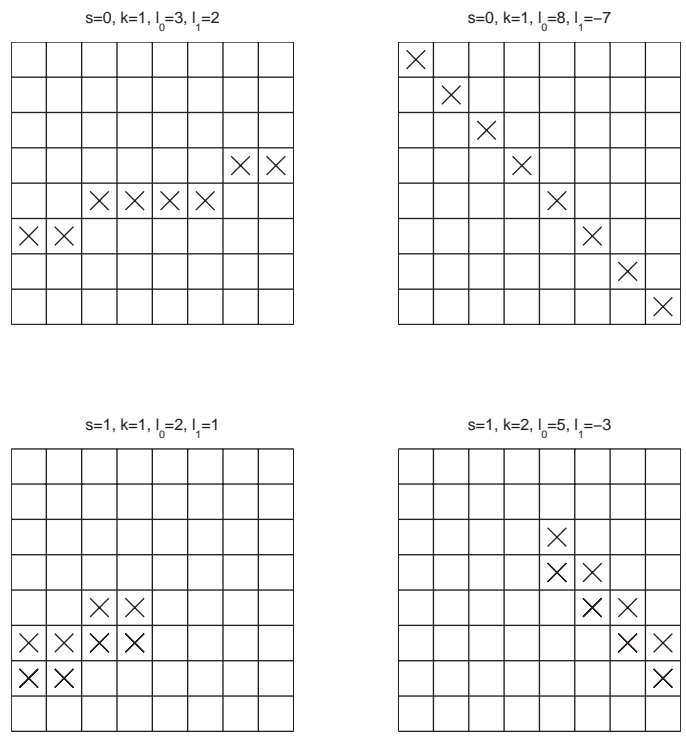


Figure 1: Four digital axoids. The marked (by \times) squares are pixels belonging to the digital axoids. The indices of these digital axoids are in the titles.

Notice that in the latter case, the value of the statistic $X(s, k, \ell_0, \ell_1)$ tends to be large.

A graph can be constructed. Let each digital axoid be a vertex. With a little bit abuse of the notation, we call it vertex $a(s, k, \ell_0, \ell_1)$. Two vertices are connected if and only if

1. they are at the same scale,
2. they are geometrically connected, and
3. they have similar slopes.

More details on the second point will be given in Section 3.4. Assign an edge between any pair of connected vertices. A graph is formed for all digital axoids.

Suppose that there is a prescribed constant N^* , such that a vertex is significant if and only if

$$X(s, k, \ell_0, \ell_1) > N^*.$$

A *significance graph* includes all the significant digital axoids and the edges connecting them. For a scale s , let $S(s)$ denote the significance graph at this scale.

An illustration of a significance graph is given in Figure 2, where three digital axoids are significant.

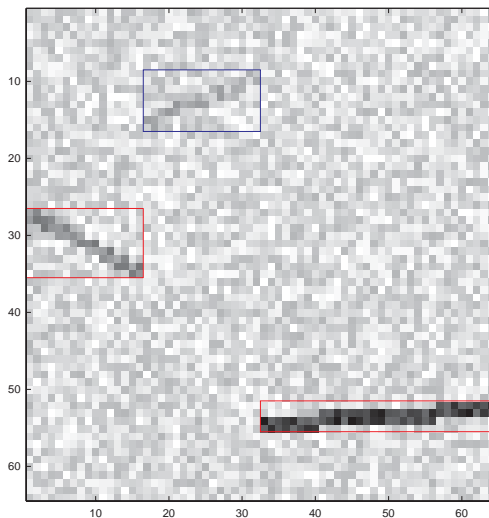


Figure 2: Illustration of a significance graph, having four vertices (i.e. significant digital axoids) and two are connected.

3.4 Good Continuation

We used the continuation (i.e. connectedness) in the graphic structure. Let ℓ_2 be another integer, $1 \leq \ell_2 \leq n$, the following two digital axoids are connected:

$$a(s, k, \ell_0, \ell_1), \quad a(s, k + 1, \ell_0 + \ell_1, \ell_2 - (\ell_0 + \ell_1)).$$

This is a case of *continuation*.

The above condition will be modified in two ways.

1. First of all, the tail (i.e. the right side) of one digital axoid may not be the exact beginning (i.e. the left side) of another digital axoid.
2. The slopes of two digital axoids (which is controlled by ℓ_1) need to be close.

Later, one may observe that this modification will influence the type of the features that are detectable. Formally, for a prescribed constants K_1 and K_2 , one has *good continuation* between axoid $a(s, k, \ell_0, \ell_1)$ and the following set of axoids:

$$a(s, k + 1, \ell_0 + \ell_1 + c_1, \ell_1 + c_2),$$

where indices c_1 and c_2 satisfy the following conditions:

$$\begin{aligned} -K_1 \leq c_1 \leq K_1, \quad 1 \leq \ell_0 + \ell_1 + c_1 \leq n, \quad \text{and} \\ -K_2 \leq c_2 \leq K_2, \quad 1 \leq \ell_0 + 2\ell_1 + c_1 + c_2 \leq n. \end{aligned}$$

The above conditions will guarantee that the second axoid is meaningful.

Examples of axoids presenting (or not presenting) good (respectively, bad) continuation are given in Figure 3 (respectively, 4).

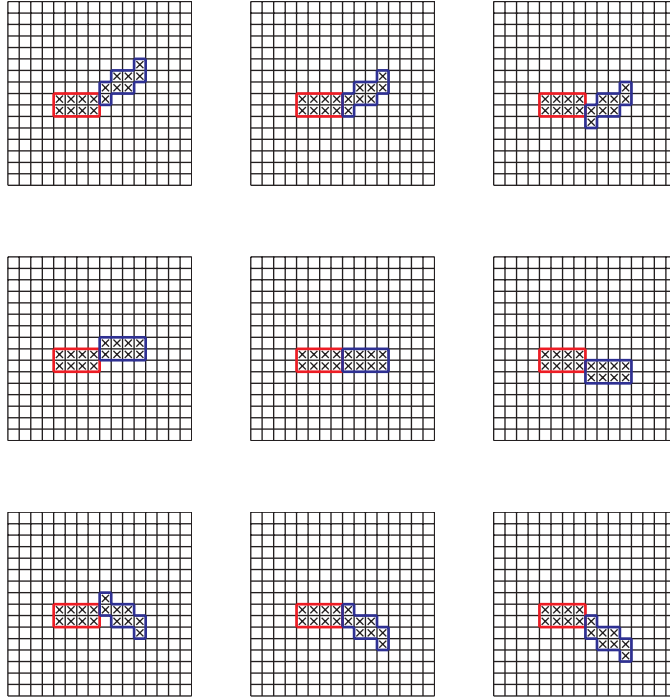


Figure 3: Cases of *good continuation*. Each row has the same amount of change of slopes. Each column has the same amount of vertical shifting.

In a significance graph, a two axoids are connected by an edge if and only if the good continuation condition is satisfied.

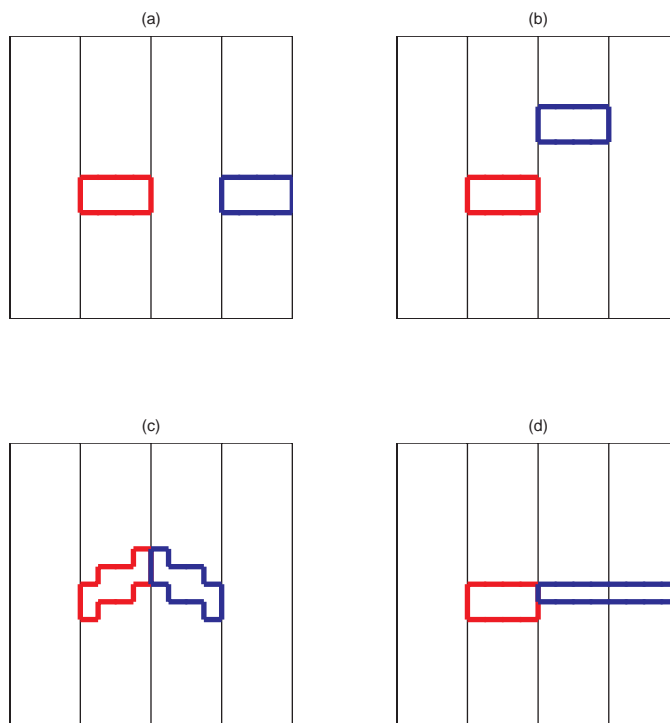


Figure 4: Cases of *bad continuation*: (a) and (b), separated axoids; (c) excessive change of slope; (d) not in the same scale.

3.5 Longest Run

For a fixed scale s , there will be a significance graph, which contains a longest chain of connected significant axoids. Such a chain of axoids is called a *longest run*. At scale s , let $R(s)$ denote a longest run. The number of axoids in $R(s)$ will be denoted by $|R(s)|$. An illustration of a significance graph and its longest run is given in Figure 5.

4 Testing Presence of Filamentary Features

The following hypotheses testing problem is considered:

$$\begin{aligned}
 H_0 &: \quad \forall(i, j), x(i, j) \sim N(0, 1), \quad \text{and} \\
 H_a &: \quad \exists F, A_n > 0, \text{ such that (1) is true.}
 \end{aligned}$$

When H_0 is true, the image is made by white noises. When H_a is true, there is an underlying feature embedded.

The testing procedure contains the following steps.

1. Compute $X(s, k, \ell_0, \ell_1)$ for all appropriate indices s, k, ℓ_0, ℓ_1 .
2. Identify the significant graph $S(s)$ at each scale.
3. Find the longest path $R(s)$.

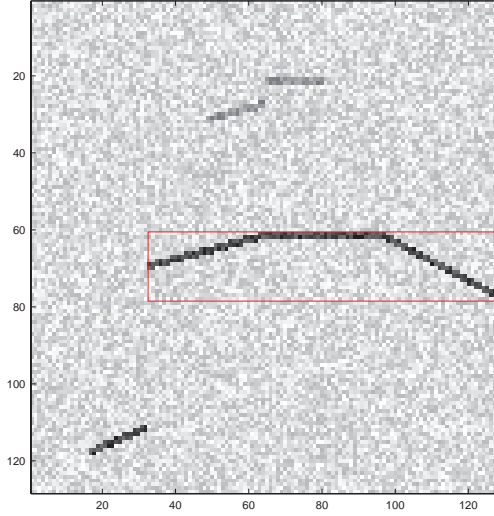


Figure 5: An example of a longest run. There are six vertices (i.e. significant digital axoids). The longest run contains three vertices.

4. Compute the overall length of the longest paths:

$$L^o = \max_s |R(s)|.$$

5. Make a decision according to the following rules:

- if $L^o > L^*$, where L^* is a prescribed number, then reject the null hypothesis H_0 ;
- if $L^o \leq L^*$, accept the null hypothesis H_0 .

By rejecting the null hypothesis, we conclude that there is sufficient evidence for the presence of an underlying feature; and vice versa.

Note that the above procedure is nearly parallel to the procedure in the paper [2].

4.1 Calibrate the N^*

Recall that in determining the significance graph, a parameter N^* is used (see Section 3.3). Recall that in [2], the key idea in determining the quantity N^* is to realize the following inequality:

$$P\{X(s, k, \ell_0, \ell_1) > N^*\} \leq \frac{p_0}{K_1 K_2},$$

where p_0 is a probability and constants K_1 and K_2 are introduced in Section 3.4. Since under the Null hypothesis, we have

$$X(s, k, \ell_0, \ell_1) \sim N(0, 1).$$

One can derive the following,

$$N^* = \Phi^{-1} \left(1 - \frac{p_0}{K_1 K_2} \right), \quad (2)$$

where Φ^{-1} is the inverse of the cumulative distribution function of the standard normal distribution.

The above way of choosing quantity N^* has some theoretical optimality, as described in [2]. In simulations, a slightly smaller value for N^* may be more advantageous. Because it will lead to more significant axoids, and will allow detection of weaker underlying feature.

4.2 Calibrate the L^*

In theory, the quantity L^* is the maximum length of the longest run with a prescribed N^* and under the Null hypothesis. Such a quantity can be approximated by repeating the simulations (under H_0) for a large number of times, and take the maximum. Apparently this is a numerically expensive method.

We found in simulations that the length of the longest run closely follows a exponential distribution, with a fast dropping rate. Hence it is sensible to choose

$$L^* = C + L_{(0)}^*,$$

where C is a constant (e.g., $C = 2$ or 3) and $L_{(0)}^*$ is the maximum length of the longest runs in a few (e.g., 10 times) simulations.

4.3 Detectability Threshold, $T^*(F)$

In theory, for a fixed feature F , there will be a constant $T^*(F)$ such that

- when $A_n > T^*(F)$, the underlying feature becomes detectable;
- when $A_n < T^*(F)$, the underlying feature is too fainted to be detected.

In our framework, we can design numerical experiments to identify such a threshold.

5 Simulations

5.1 Synthetic Data

Synthetic data are used in the simulations. We describe four types of geometric objects, which are representative on the filamentary features that are of interests.

1. *Trigonometric Functions.* Consider a function in a unit square:

$$y = 0.5 + \frac{(1 - \delta_2)}{2} \sin[2\pi(1 + \delta_1)(x - 0.5)],$$

where $x \in (0.5 - 0.5/(1 + \delta_1), 0.5 + 0.5/(1 + \delta_1))$, and δ_1 and δ_2 are two constants: e.g., $\delta_1 = 0.5$ and $\delta_2 = 0.2$. A pixel (i, j) intersects with the above function if and only if the square $[(i - 1)/n, i/n] \times [(j - 1)/n, j/n]$ intersects with the above function. A feature F is made by all such pixels. An illustration of such a feature is given in Figure 6 (a).

2. *Thickened Trigonometric Functions.* The above feature can be ‘thickened’ by gluing the pixels immediately above or below into the feature. An illustration is given in Figure 6 (b).

3. *Beams*. We consider the function in a unit square:

$$y = 0.5 + a(x - 0.5),$$

where $x \in (0.5 - 0.5\delta_3, 0.5 + 0.5\delta_3)$. The following parameters may be chosen: $\delta_3 = 0.8$, $a = 1, 1/2, 1/4, \dots$. The feature F is made by pixels that intersect the above function. An illustration is given in Figure 6 (c).

4. *Thickened Beams*. Again by gluing pixels immediately above and below a digital beam, we have a thickened beam. Let t denote the thickness (i.e., the number of pixels vertically aligned in a flat portion of the underlying feature). We may choose $t = 2, 4, 8$, etc. An illustration is given in Figure 6 (d).

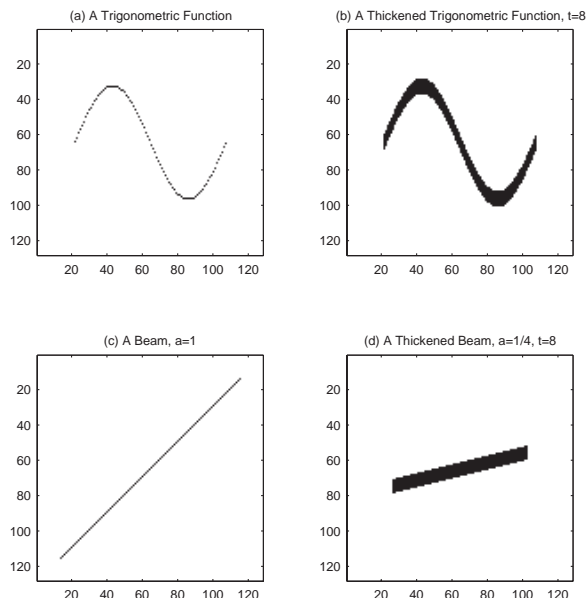


Figure 6: Features that are used in the numerical experiments.

5.2 Simulations

For a fixed value n , the threshold N^* is given by (2) (where we choose $p_0 = 1/2$, $K_1 = 2^s$, $K_2 = 2 \cdot S \cdot n/2^s$, and $S = 4$ is the maximum slope). The Table 1 gives a list of values of N^* that are used.

Table 1: Values of N^* .

$n =$	32	64	128	256	512	1024
$N^* =$	2.8856	3.0973	3.2972	3.4871	3.6683	3.8419

The threshold L^* is determined by simulations: $L^* = 2 + L_{(0)}^*$, where the quantity $L_{(0)}^*$ is the maximum length of the longest runs in ten simulations. The Table 2 gives the values of $L_{(0)}^*$ and L^* for a range of n 's.

Table 2: Determining the values of L^* .

$n =$	32	64	128	256
$L_{(0)}^* =$	2	2	4	2
$L^* =$	4	4	6	4

The computing times for simulations in MATLAB at various sample sizes are given in Table 3.

Table 3: Computing time (in seconds) for each simulation.

$n =$	32	64	128	256
Computing Time	2.87	20.54	154.36	1264.8

For a given feature, e.g. a trigonometric function, one would like to know how large should the value of A_n be such that the underlying feature F can be reliably detected. For a fixed F (which is the first synthetic signal in Figure 6) and a fixed $n = 64$, applying N^* and $L^*(= 4)$ that are given above, Table 4 gives the numbers of detection out of 10 simulations. Figure 7 presents the noisy images with various amplitudes (A_n 's).

Table 4: Detections out of 10 simulations for a trigonometric curve while $n = 64$ and $t = 1$.

$A_n =$	0	2.000	2.333	2.666	3.000	4.000
Detected Cases	0	0	4	7	9	10

5.3 More Observations

5.3.1 Increased sample size for the trigonometric features

In another set of the experiments, the sample size is increased to 128×128 . For different amplitudes A_n , the number of detections among 10 simulations are reported in Table 5. It is shown that when amplitude increased from $1/4$ to $1/2$, the underlying feature becomes detectable. Figure 8 presents the random images with the first three amplitudes that are used in Table 5. Notice that when $A_n = 0.5$, the underlying feature is still obscure, but the detection rate is nearly 100%.

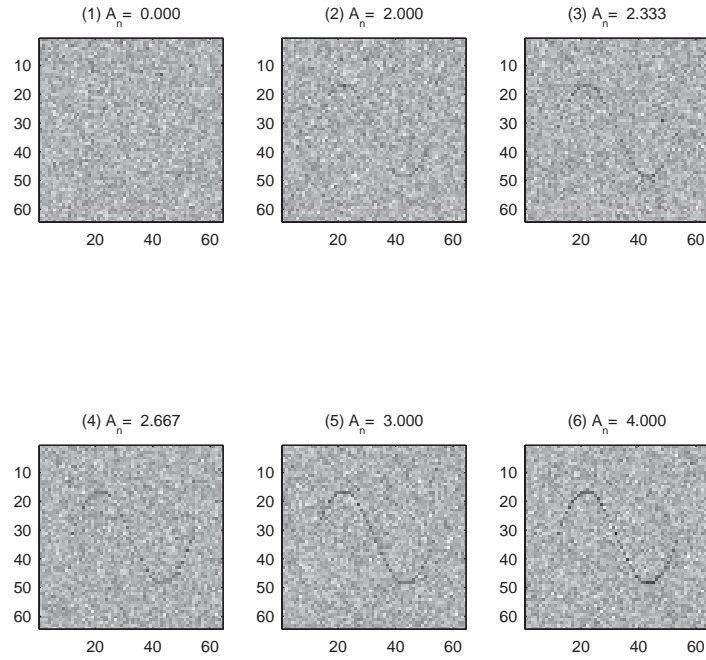


Figure 7: Noisy images with an underlying trigonometric curve having a range of amplitudes (provided in the titles). It shows that the proposed method can detect an underlying feature which is not obviously visible: case (5). Refer to Table 4.

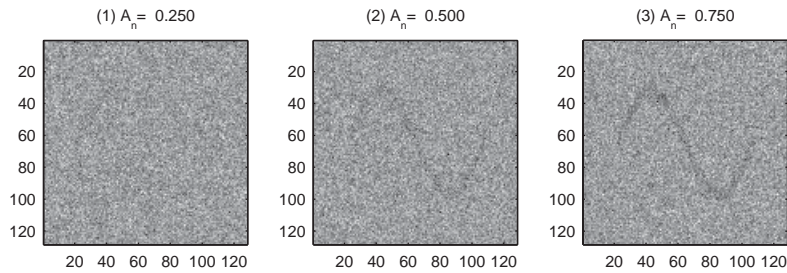


Figure 8: The random images that are used in the experiments that are reported in Table 5. The thickness of the underlying feature is $t = 8$.

Table 5: Detections out of 10 simulations for a trigonometric curve while $n = 128$ and $t = 8$.

$A_n =$	1/4	1/2	3/4	1
Detected Cases	0	10	10	10

5.3.2 Thinner objects

For an underlying trigonometric curve, when the sample size is still $n = 128$, however the thickness is reduced to $t = 1$, Table 6 presents the detection rates with a range of A_n 's. Figure 9 presents some boundary cases.

Table 6: Detections out of 10 simulations for a trigonometric curve while $n = 128$ and $t = 1$.

$A_n =$	1	2	3	4
Detected Cases	0	3	10	10

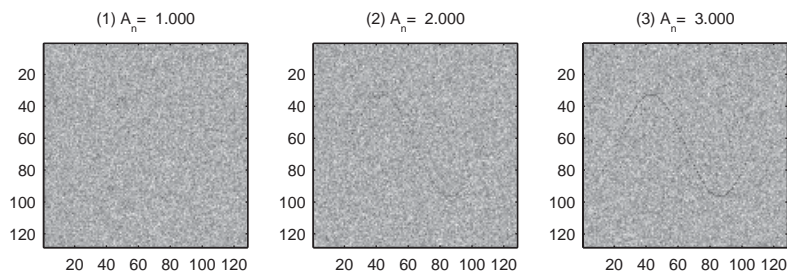


Figure 9: The random images that are used in the experiments that are reported in Table 6. The thickness of the underlying feature is reduced to $t = 1$.

5.4 Longest Runs

A key motivation of the proposed method is that the lengths of the longest runs are significantly larger when there are underlying features. Figure 10 illustrate this by presenting two comparison cases.

6 Conclusion

We present a method which is theoretically optimal and practically capable of detecting curvilinear features with arbitrary positions, orientations, anisotropic ratios, and smoothness. The proposed framework works for digital imageries. Simulations demonstrate the

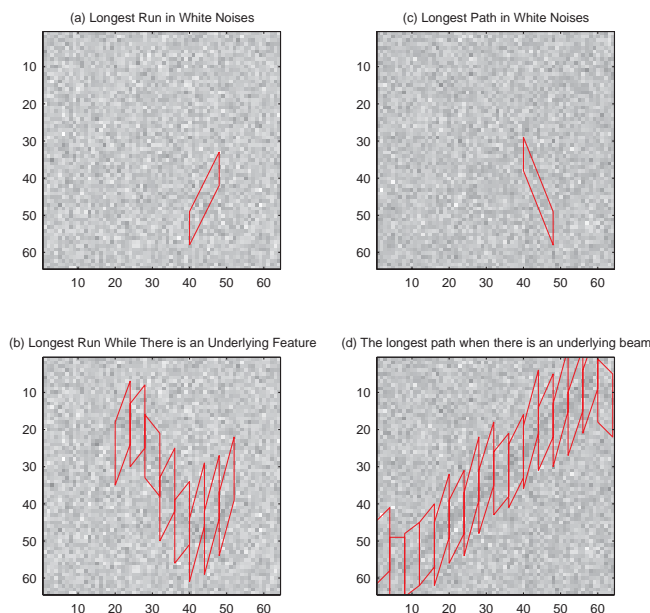


Figure 10: Illustration of an increment of length of the longest run when an underlying feature (a trigonometric function for (a) and (b), and a beam for (c) and (d)) is present. When there is an underlying feature, the length of the longest run is significantly larger.

effectiveness of the algorithms. The future works include examining the variations in designing the digital axoids, and their impact on the efficiency and detection sensitivity of the proposed methodology.

References

- [1] E. Arias-Castro, D.L. Donoho, and X. Huo (2003). Asymptotically optimal detection of geometric objects by fast multiscale methods. Working paper.
- [2] E. Arias-Castro, D.L. Donoho, and X. Huo (2003). Adaptive multiscale detection of filamentary structures embedded in a background of Uniform random points. Working paper.
- [3] E. Arias-Castro, D.L. Donoho, X. Huo, and C. Tovey (2003). Connect-The-Dots: How many random points can a regular curve pass through? (Work in progress.)
- [4] D.L. Donoho and X. Huo (2002). *Beamlets and multiscale image analysis*. In: T.J. Barth, T. Chan, and R. Haimes (Eds.), Springer Lecture Notes in Computational Science and Engineering 20, 149-196.